

## Imaging the Surface and the Interface Atoms of an Oxide Film on Ag{111} by Scanning Tunneling Microscopy: Experiment and Theory

C. I. Carlisle, and D. A. King

*Department of Chemistry, University of Cambridge, Lensfield Road, Cambridge, CB2 1EW, United Kingdom*

M.-L. Bocquet,<sup>1</sup> J. Cerdá,<sup>2</sup> and P. Sautet<sup>1</sup>

<sup>1</sup>*Institut de Recherches sur la Catalyse, CNRS, 2 Avenue A. Einstein, F-69626 Villeurbanne Cedex, France and Laboratoire de Chemie Theorique, Ecole Normale Supérieure, F-69364 Lyon Cedex 07, France*

<sup>2</sup>*Instituto de Ciencia de Materiales de Madrid, CSIC, Cantoblanco, 28049 Madrid, Spain*

(Received 22 October 1999)

High-resolution images of the vacuum oxide surface atomic structure of Ag{111}- $p(4 \times 4)$ -O reveal large terraces of a perfect  $(4 \times 4)$  reconstruction. Under certain conditions, the surface Ag atoms at the interface between the reconstructed oxide layer and the underlying Ag{111} lattice are also imaged, providing the structural registry. Scanning tunneling microscopy simulations reveal a strong sensitivity to structure and comparison with the experimental images, therefore providing an atom-by-atom model for the entire metal-oxide-vacuum structure.

PACS numbers: 82.65.Jv, 61.16.Ch, 79.20.Rf, 82.65.My

The derivation of crystallographic structures from atomic-scale scanning tunneling microscopy (STM) studies is developing rapidly [1]. The simulation of images using reliable techniques has advanced to the determination of site symmetry for submonolayer structures from molecular and atomic adsorbates [2,3]. However, thin films, such as oxides on metals [4], present particular challenges; in particular, the registry with the underlying substrate has not previously been directly imaged.

We present the first atomic resolution STM images of the Ag{111}- $p(4 \times 4)$ -O reconstruction along with atomic images of the interface between this and the underlying Ag{111} lattice, and the top-layer images are compared with theoretical simulations. The oxide structure is similar to that originally proposed by Rovida *et al.* [5], but with missing Ag<sup>+</sup> ions.

The oxygen-promoted reconstruction of the Ag{111} surface is of significance to the catalytic oxidation of organic molecules. Ag{111} is the predominant face present in supported catalysts [6] and powders [7] and is inert to dissociative adsorption in the absence of oxygen. Silver is used, in particular, as a catalyst in the oxidation of ethylene to epoxide [8] and reactions of organic molecules with oxygen precovered Ag{111} and has already been subjected to many studies [9]; yet an atomic-scale description of these reactions is still lacking. The present paper is a first step towards this complete description.

The structure has previously been investigated by low energy electron diffraction (LEED) [5,10,11], high-resolution electron energy loss spectroscopy (HREELS) [11], x-ray photoelectron spectroscopy (XPS) [11–13], temperature programmed desorption (TPD) [10–14], mixed beam thermal energy atom scattering (MBTEAS) [14], and nuclear reaction analysis (NRA) [11]. At temperatures between 400 and 500 K, the chemisorption

of atomic oxygen on Ag{111} produces a  $p(4 \times 4)$  LEED pattern over a range of coverages up to a saturation of  $0.51 \pm 0.04$  ML (monolayer) [13]. This structure has been interpreted in terms of a single O-Ag-O trilayer of Ag<sub>2</sub>O in the  $\langle 111 \rangle$  direction epitaxed to the Ag{111} surface shown in Fig. 1(A). Figure 1(B) shows a variation of this model, which is tested in the present study.

The experiments were carried out using an Omicron Low-Temperature STM at a base pressure of  $1 \times 10^{-10}$  mbar and optimized for operation at 4 K, with the additional capability of working at 77 K and room temperature. The crystal was cleaned by repeated argon ion sputtering at 600 K followed by 780 K anneal cycles. Since the dissociative sticking probability of O<sub>2</sub> on Ag{111} is very low, the oxide  $(4 \times 4)$  structure was prepared by the alternative technique of Bare *et al.* [11], using a 600 L [1 langmuir (L) =  $10^{-6}$  Torr s] dose of NO<sub>2</sub> at a sample temperature of 490 K, which produced a sharp LEED pattern.

In Fig. 2 we display a superposition of three 4 K STM images, one from clean Ag{111} (A) and two from the  $p(4 \times 4)$ -O structure obtained under different imaging conditions (B and C). The clean surface atomically resolved image shown was chosen because it displays inverted contrast, in which the Ag atoms appear as depressions (dark areas); image C also shows top {111} layer Ag atoms with inverted contrast. The sign of the contrast is determined by the state of the tip and can change during scanning [15].

Image B is a high-resolution image of the reconstructed surface. This  $(4 \times 4)$  structure covers large areas of the surface and exhibits remarkably few defects, with no domain boundaries or misfit dislocations within terraces. The bright features, in a honeycomb arrangement, are 6.7 Å apart and the image shows a maximum corrugation

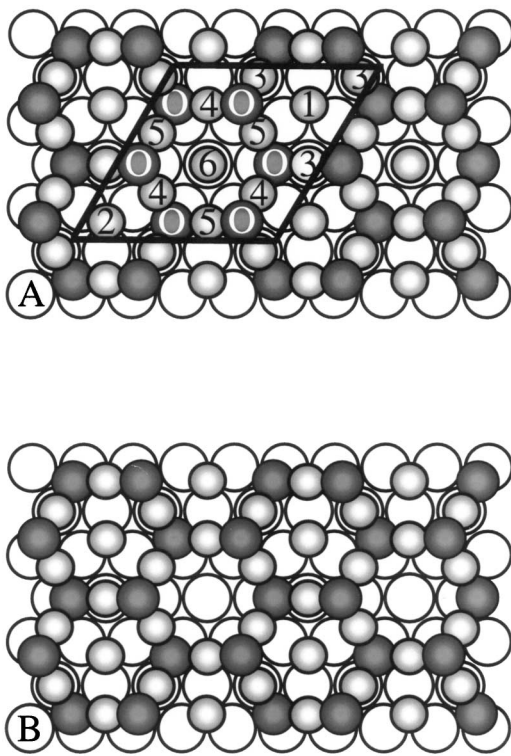


FIG. 1. (A)  $\text{Ag}_2\text{O}$  trilayer structure epitaxially grown on  $\text{Ag}\{111\}$  as proposed by Rovida *et al.* [3]. Light shaded spheres correspond to Ag atoms and dark shaded spheres correspond to O atoms in the trilayer. Open circles indicate the position of the underlying surface  $\text{Ag}\{111\}$  layer. Within the marked unit cell, Ag atoms that are symmetry equivalent have been labeled with the same number. (B) The new model of the Ag-deficient trilayer of  $\text{Ag}_{1.83}\text{O}$  epitaxially grown on the  $\text{Ag}\{111\}$  substrate.

amplitude of between 0.4 and 1.2 Å, depending on tip-to-sample separation. Tip-to-sample biases were varied between  $-2$  and  $+2$  V and yielded the same image.

At very low gap resistances (200 k $\Omega$ ) we observe a superposition of both the reconstruction image and a  $1 \times 1$  array that is associated with the underlying  $\text{Ag}\{111\}$  top layer, shown as C in Fig. 2. It provides directly in real space the registry between the bright features of the oxide layer and threefold hollow sites of the underlying  $\text{Ag}\{111\}$ . This latter image requires a very short tip-sample distance that implies significant forces in the tunnel junction. The underlying  $\text{Ag}\{111\}$  surface always presents inverted contrast, as in image A. This extreme regime is well out of the reach of understanding with our simulation tool described below.

The theoretical STM image simulations have been performed employing a Green's-function-based scattering formalism that allows a realistic atom-by-atom structural description of the entire STM interface (surface and tip apex) [2]. For all of the images, shown below, we have modeled the tip as an isolated (i.e., nonperiodic) pyramid of 5 W atoms stacked on top of a W{110} surface. In addition, we have tested a blunt tip (a 4 W atom tetrahedron stacked on top of a W{111} surface), together with a tip

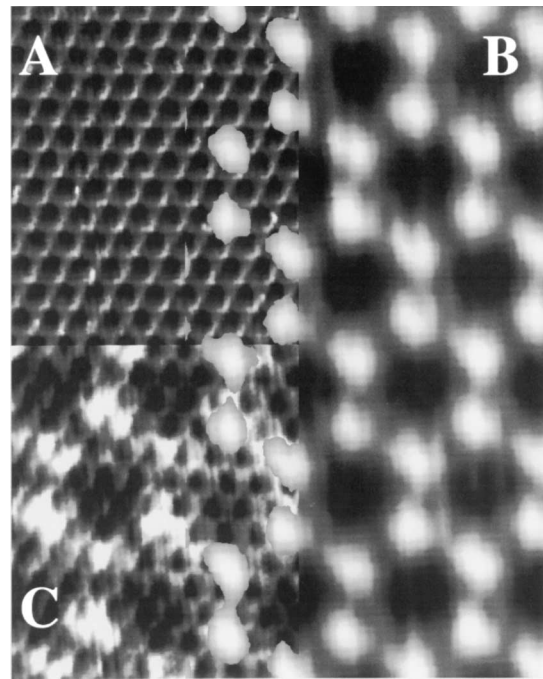


FIG. 2. A superposition of atomic resolution STM images showing (A) an inverted contrast image from clean  $\text{Ag}\{111\}$ , (B) a surface image of the  $(4 \times 4)\text{-O}$  structure, and (C) an interface image of the  $(4 \times 4)\text{-O}$  structure. The overall size of the image is  $52 \text{ \AA} \times 65 \text{ \AA}$ . The images were obtained under the following conditions. (A) 4 K, with a bias voltage of 5 mV and a tunneling current of 1.7 nA. (B) 298 K, with a bias voltage of 5 mV and a tunneling current of 0.103 nA in constant current mode. (C) 4 K, with a bias voltage of 5 mV and a tunneling current of 1.9 nA in constant height mode.

of a different chemical identity (a 4 Pt atom tetrahedron on top of a Pt{111} surface).

The electronic structure for the system has been approximated using a Hückel type Hamiltonian where the atomic orbital parameters involved (wave functions and on-site energies) have been optimized after least-squares fits of the bulk energy bands to accurate *ab initio* ones [16]. In particular, the parameters for the Ag and O atoms in the trilayer were fitted to the oxide bulk bands, while those for the Ag, W, and Pt atoms in the substrate and tip bulk result from a fit to their respective bulk bands. The quality of the fits is mirrored by root mean square deviations below 110 meV for all elements considered in this work. Moreover, we have found no qualitative changes in the shape of the calculated images with small modifications of these parameters.

For the actual evaluation of the tunneling current, and in order to include the contribution of any possible surface states, we have replaced the Landauer-Bütticker formalism employed in previous work by the formula of Todorov [17]. The  $t$ -matrix has been evaluated only up to first order in the tip-surface interactions, although we have checked that for the tip-sample distances considered, multiple-scattering corrections are negligible.

Four theoretical simulations of trial structures are presented in Fig. 3. We show only the results for the  $W\{110\}$  tip, since the images are qualitatively similar for the other tip structures considered in this work. Model A is identical to that in Fig. 1(A). The following two models are variations on this: Model B is a modification of model A, obtained by removing the Ag atoms labeled “6,” and is shown as structure B in Fig. 1; model C is similar to model A after the removal of Ag 6 but also with the silver atoms “1” and “2” replaced by oxygen atoms. Model C has been chosen as a possible realistic structure with an oxygen coverage of 0.5 ML, as measured by NRA [13]. Since we need, as input data, the coordinates of all constituent atoms of the sample, standard atomic distances have been considered for the geometry of the metal-oxide interface. Hence, we have assumed a considerable reconstruction of the trilayer in order to preserve typical bond distances both for Ag-O [ $d_{(\text{Ag-O})} = 2.05 \text{ \AA}$ ] and Ag-Ag [ $d_{(\text{Ag-Ag})} = 2.90 \text{ \AA}$ ]. This requirement leads to a large buckling of the Ag within the overlayer, Ag “3” and Ag 6 being positions  $0.5 \text{ \AA}$  higher than the other Ag surface atoms.

For completeness, we have also considered model D, in which individual oxygen atoms are chemisorbed on a clean  $\text{Ag}\{111\}$  surface in the threefold hollow positions where the bright features are observed in Fig 2(C) (equivalent to Ag atom positions 1 and 2).

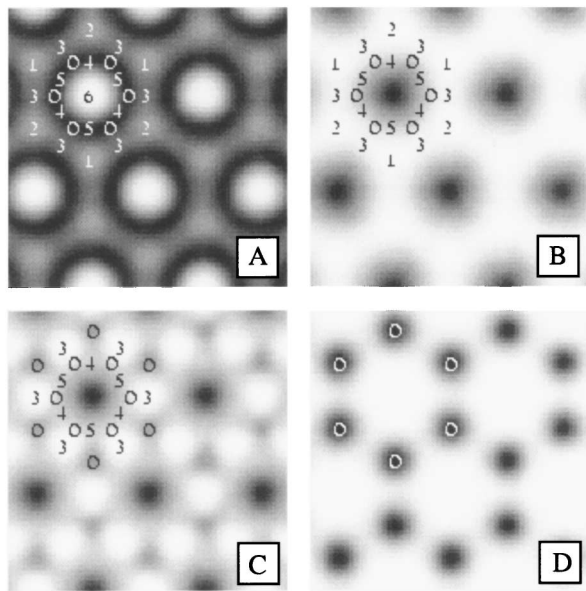


FIG 3. Topographic STM images ( $28 \text{ \AA} \times 28 \text{ \AA}$ ), calculated for the four models explained in the text. Tunneling conditions:  $V = -25 \text{ mV}$ ,  $I = 2 \text{ nA}$ . Within each image, the numbering of the positions of the Ag atoms at the trilayer follows that given in Fig. 1(A) while O indicates the location of the oxygen atoms. All images shown were calculated with a  $W\{110\}$  tip. Model A, maximum corrugation amplitude (MCA) =  $0.67 \text{ \AA}$ ; model B, MCA =  $1.24 \text{ \AA}$ ; model C, MCA =  $1.02 \text{ \AA}$ ; model D, MCA =  $0.35 \text{ \AA}$ .

As a first conclusion we discard models A, C, and D as, by inspection of Figs. 2 and 3, the simulated patterns are inconsistent with that observed. In contrast, model B quite closely resembles the experimental image and provides the basis for an improved structural model. However, the calculated image in Fig. 3(B) is not in full agreement with experiment, with insufficient contrast between Ag 3 and the Ag atoms at 1 and 2. We have therefore considered two refinements of model B: (i) decreasing the buckling imposed on the oxide overlayer by relaxation of the substrate below the oxide, model B'; (ii) creating vacancies, model B''.

The first modification of model B is simply to bring the Ag 3 atoms closer to the  $\text{Ag}\{111\}$  surface by setting an adsorption height for Ag 3 of  $2.6 \text{ \AA}$  (instead of  $2.9 \text{ \AA}$  in model B). However, this model yields a bonding distance which is too small between Ag 3 and the substrate atom directly below [ $d_{(\text{Ag } 3\text{-Ag})} = 2.6 \text{ \AA}$ ]. This distance may be increased by including a normal displacement of the substrate atom into the bulk. Indeed, we have found that the calculated STM image is unchanged after considering an inward relaxation of  $0.2 \text{ \AA}$  at the  $\text{Ag}\{111\}$  surface corresponding to a value of  $d_{(\text{Ag } 3\text{-Ag})} = 2.8 \text{ \AA}$ , much closer to the bulk interatomic distance of  $2.90 \text{ \AA}$ . In-plane displacements for any of these two silver atoms have not been considered since they are not consistent with the threefold symmetry imposed on all models. The calculated images for this new model are shown in Figs. 4(B'<sub>1</sub>) and (B'<sub>2</sub>) for both a  $W\{110\}$  and a  $W\{111\}$  tip, respectively (the  $\text{Pt}\{111\}$  tip result is not shown since it is essentially the same as the  $W\{110\}$  tip). As expected, the resulting simulated images are very similar to the experimental image of Fig. 2(B).

The second modification of model B involves removal of the substrate atoms below Ag 3. These periodic vacancies in the first layer of the Ag substrate allow the removal of the buckling at the oxide layer, so that its structure is essentially that of the bulk  $\text{Ag}_2\text{O}$  oxide. The calculated images shown in Figs. 4(B''<sub>1</sub>) and (B''<sub>2</sub>), for  $W\{110\}$  and  $W\{111\}$  tips, respectively, also present good agreement with the experiment. However, the images calculated with sharp tips (i.e.,  $W\{110\}$  and  $\text{Pt}\{111\}$ , images for the latter not shown) present a rather triangular shape for the bumps which are not found experimentally.

We conclude that the only model compatible with the experimental images is model B', the  $\text{Ag}^+$  deficient oxide trilayer model with a reduced adsorption height for the Ag 3 overlayer atoms; the corresponding simulations are shown in Figs. 4(B'<sub>1</sub>) and (B'<sub>2</sub>). In this model the contrast is very clear with the presence of Ag 1 and 2 dominating the image to such an extent that the remaining oxide structure is unresolved. The maximum corrugation amplitude  $1.21 \text{ \AA}$  is very close to the maximum experimental value of  $1.2 \text{ \AA}$ .

A final interesting point to note is that the STM is highly sensitive to the chemical environment of the outer

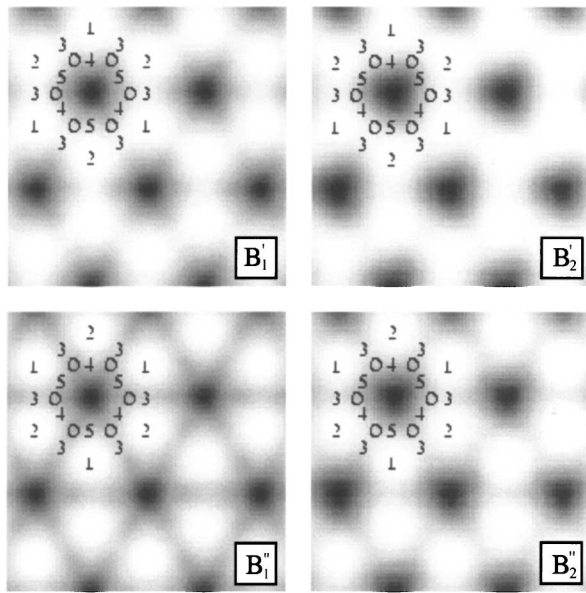


FIG. 4. Images calculated from two modifications of Model B using two different tip structures: ( $B'_1$ )  $W\{110\}$  tip, MCA = 1.21 Å; ( $B'_2$ )  $W\{111\}$  tip, MCA = 0.76 Å; ( $B''_1$ )  $W\{110\}$  tip, MCA = 1.16 Å; ( $B''_2$ )  $W\{111\}$  tip, MCA = 0.74 Å.

Ag atoms in the trilayer. Hence, the Ag at the center of the O-Ag-O rings (positions 1 and 2) appears much brighter than Ag included in the rings themselves, despite having a lower  $z$  coordinate. We have therefore performed a theoretical analysis of the tunneling current in order to show that the electronic origin is twofold. First, Ag atoms 1 and 2 show an increased density of states at the Fermi level, where the main contribution arises from the  $s$  orbital of the Ag 1 and 2 atoms. Second, at these bright positions, the current contribution is enhanced by constructive interference in the tip and sample orbital couplings, whereas the interference is far smaller for the Ag 3 in the O-Ag-O arrangement because of out-of-phase contributions from the  $p_z$  orbital of neighboring upper oxygens.

In conclusion, we have, through a combined experimental and theoretical study, deduced the structure of the  $Ag\{111\}$ - $p(4 \times 4)$ -O phase. The simulations show that the technique is very sensitive to the electronic structure and coordination of surface atoms, and hence to different surface oxide terminations. The registry between the oxide layer and the underlying lattice has provided an essential starting point for the proposal of several possible models from which the theoretical simulations have been produced. Simulations demonstrate that only those outer Ag atoms not directly connected to oxygen atoms are resolved in the experimental image. The key factor in reproducing

the corrugated bumps in the honeycomb array turns out to be a moderate buckling of the  $z$  coordinates between the two types of outer Ag atoms (Ag 1–2 and Ag 3). However, the exact atomic coordinates await either a LEED intensity analysis or density functional theory calculations, since we are at the limit of current STM theory. We hope this contribution will stimulate further use of the combined experiment and/or theory approach to STM analyses, primarily in determining models for other complex reconstructions.

We acknowledge EPSRC for an equipment grant and a research grant (C.I.C.) and Johnson Matthey for additional financial support. Dr. W.S. Sim and Dr. T. Fujimoto are thanked for assistance with the experiments. M.L.B., J.C., and P.S. acknowledge support from the Spanish-French collaboration program PICASSO 98045. J.C. also acknowledges a grant from the Spanish CICYT program PB96-0916.

- [1] J.C. Dunphy, P. Sautet, D.F. Ogletree, and M. Salmeron, *Phys. Rev. B* **52**, 11 446 (1995).
- [2] M.O. Pedersen, M.-L. Bocquet, P. Sautet, E. Lægsgaard, I. Stensgaard, and F. Besenbacher, *Chem. Phys. Lett.* **299**, 403 (1999); M.-L. Bocquet, J. Cerdá, and P. Sautet, *Phys. Rev. B* **59**, 15 437 (1999).
- [3] J. Cerdá, M. A. Van Hove, P. Sautet, and M. Salmeron, *Phys. Rev. B* **56**, 15 885 (1997); **56**, 15 900 (1997).
- [4] H. Galloway, P. Sautet, and M. Salmeron, *Phys. Rev. B* **54**, R11 145 (1996).
- [5] G. Rovida, F. Pratesi, M. Maglietta, and E. Ferroni, *Surf. Sci.* **43**, 230 (1974).
- [6] M. Dean and M. Bowker, *Appl. Surf. Sci.* **35**, 27 (1988).
- [7] M. Bowker, P. Pudney, and G. Roberts, *J. Chem. Soc. Faraday Trans. 1* **85**, 2635 (1989).
- [8] R. A. Van Santen and H.P.C.E. Kuipers, *Adv. Catal.* **35**, 265 (1987).
- [9] W.S. Sim, P. Gardner, and D.A. King, *J. Am. Chem. Soc.* **118**, 9953 (1996); W.S. Sim and D.A. King, *J. Phys. Chem.* **100**, 14 794 (1996).
- [10] C.T. Campbell, *Surf. Sci.* **157**, 43 (1985).
- [11] S.R. Bare, K. Griffiths, W.N. Lennard, and H.T. Tang, *Surf. Sci.* **342**, 185 (1995).
- [12] R. B. Grant and R. M. Lambert, *Surf. Sci.* **146**, 256 (1984).
- [13] V.I. Bukhtiyarov, V.V. Kaichev, and I.P. Prosvirin, *J. Chem. Phys.* **5**, 2169 (1999).
- [14] A. Raukema, D. A. Butler, F. M. A. Bor, and A. W. Kleyn, *Surf. Sci.* **347**, 151 (1996).
- [15] C. J. Chen, *J. Vac. Sci. Technol. B* **12**, 2193 (1994).
- [16] J. Cerdá and F. Soria, *Phys. Rev. B* (to be published).
- [17] T.N. Todorov, G. A. D. Briggs, and A. P. Sutton, *J. Phys. Condens. Matter* **5**, 2389 (1993).